DOI:
10.1016/j.hrthm.2019.11.013

Document Version
Peer reviewed version

Evaluation of the Re-entry Vulnerability Index to Predict Ventricular Tachycardia Circuits Using High Density Contact Mapping

Michele Orini PhD[1,2], Adam J. Graham MD[3], Neil T. Srinivasan MD PhD[3], Fernando O. Campos PhD[4], Ben M. Hanson PhD[5], Anthony Chow MD FRCP[3], Ross J. Hunter MD[3], Richard J. Schilling MD FRCP[3], Malcolm Finlay MD PhD[1,3], Mark J. Earley MD FRCP[3], Simon Sporton MD FRCP[3], Mehul Dhinoja MD[3], Martin Lowe MD FRCP[3], Bradley Porter MD[6], Nicholas Child MD[6], Christopher A. Rinaldi MD FRCP[6], Jaswinder Gill MD FRCP[6], Martin Bishop PhD [4], Peter Taggart MD DSci[1], Pier D. Lambiase MD FHRS[1,3]

1: Institute of Cardiovascular Science, University College London, London, United Kingdom

2: The William Harvey Research Institute, Queen Mary University of London, London, United Kingdom

3: Electrophysiology Department, Barts Heart Centre, St Bartholomew's Hospital, London, United Kingdom

4: School of Biomedical Engineering and Imaging Sciences, King's College London, London, United Kingdom

5: Department of Mechanical Engineering, University College London, London, United Kingdom

6: Department of Cardiology, Guys and St Thomas' NHS Trust, London, United Kingdom

Address for correspondence:

- Professor Pier Lambiase, ICS UCL and Barts Heart Centre, London, UK: p.lambiase@ucl.ac.uk
- Dr Michele Orini, ICS UCL, London, UK : m.orini@ucl.ac.uk

Conflict of interest: none declared

Word count: 5000

Running title: RVI predicts VT exit sites during pacing

Abstract

Background: Identifying arrhythmogenic sites to improve ventricular tachycardia (VT) ablation outcomes remains unresolved. The re-entry vulnerability index (RVI) combines activation and repolarization timings to identify sites critical for re-entrant arrhythmia initiation without inducing VT.

Objective: To provide the first assessment of RVI's capability to identify VT sites of origin using high-density contact mapping and comparison with other activation-repolarization markers of functional substrate.

Methods: 18 VT ablation patients (16M, 72% ischemic) were studied. Unipolar electrograms were recorded during ventricular pacing and analysed off-line. Activation time (AT), activation-recovery interval (ARI), repolarization time (RT) were measured. Vulnerability to re-entry was mapped based on RVI and spatial distribution of AT, ARI and RT. The distance from sites identified as vulnerable to re-entry to the VT site of origin was measured, with distances <10 mm and >20 mm indicating accurate and inaccurate localization, respectively.

Results: The origin of 18 VTs was identified (n=6 entrainment, n=12 pace-mapping). RVI maps included 1012, 408—2098 (median, 1^{st}—3^{rd} quartiles) points/patient. RVI accurately localized 72.2% VT sites of origin, with median distance equal to 5.1, 3.2—10.1 mm. Inaccurate localization was significantly less frequent for RVI than AT (5.6% vs 33.3%, OR=0.12, P=0.035). Compared to RVI, distance to VT sites of origin was significantly larger for sites showing prolonged RT and ARI, and non-significantly larger for sites showing highest AT and ARI gradients.

Conclusion: RVI identifies vulnerable regions closest to VT sites of origin. Activation-repolarization metrics may improve VT substrate delineation and inform novel ablation strategies.

Keywords: Re-entry vulnerability index, activation time, repolarization time, ventricular tachycardia, ablation, substrate mapping.

Introduction

Recurrence rates of ventricular tachycardia (VT) in structural heart disease remain sub-optimal at 50% on average for a first time catheter ablation highlighting the need for more effective ablation strategies [1]. Although VT induction and activation/entrainment mapping is the preferred method to identify the circuit, this often cannot be performed due to instability of the VT itself or haemodynamic compromise [2]. Substrate ablation strategies have been proposed and are based upon electrogram features related to signal morphology or local conduction parameters [3,4].

Despite the fact that the earliest research in the field identified spatio-temporal repolarization dynamics as one of the fundamental factors modulating vulnerability to re-entry [5], current clinical practice relies almost exclusively on conduction-related parameters to identify target sites. A prerequisite for re-entry is unidirectional block whereby an activation wavefront blocks at a region of late repolarization where tissue is still refractory, circumvents the area of block through slow conducting pathways and re-enters the proximal region. The ability to re-enter the proximal region depends not only on the conduction delay around the blocked area but also on the timing of the returning wavefront relative to completion of repolarization and hence re-excitability in the proximal region [6]. This is the basis of the re-entry vulnerability index (RVI)[6,7], an activation-repolarization metric that provides a point-by-point quantification of the likelihood of re-entry and enables functional VT substrate delineation.

Previous mechanistic studies [6–9] based on ex-vivo animal data and computational models have confirmed the link between RVI and sites of VT initiation. Preliminary observations on retrospective data utilising non-contact mapping technology in selective RV disorders have shown encouraging results [10]. However, RVI's potential as a clinical tool to localize critical sites for VT initiation has never been formally assessed using state of the art high-density mapping. The aim of this study was to relate the vulnerable region delineated by RVI to the VT site of origin (VT-SoO) and compare RVI to other spatio-temporal metrics of activation and repolarization.

Methods

Concept and quantification of RVI

The RVI concept is illustrated in Figure 1. Panel A illustrates the case of bidirectional block and no re-entry: An activation wavefront (orange line) arrives at a region that is refractory and blocks (point P). The wavefront travels around the area of block (orange line) and arrives back at the distal side of the block (point D) which is still refractory and blocks in the reverse direction (bidirectional block). Bidirectional block occurs because repolarization time at point P is longer than activation time at point D. Panel B illustrates the case where re-entry occurs. The returning wavefront arrives back at the initial site of block (point D) when the region proximal to it has regained excitability. The returning wavefront is now able to propagate back to the proximal region and complete a re-entrant circuit. Re-entry occurs because repolarization time at point P is shorter than activation time at point D. The re-entry vulnerability index (RVI) is represented by the interval between activation time at the distal site D and repolarization at the proximal site P, i.e. RT_P-AT_D, shown as shaded areas in Figure 1. A shorter RVI (panel B) is more likely to be associated with re-entry than a longer RVI (panel A).

Patients and procedures

Patients with structural heart disease undergoing catheter ablation for VT were prospectively recruited at the Barts Heart Centre and St Thomas's Hospital, London, UK. Patients gave informed consent for inclusion into VT mapping research approved by local REC. Cardiac mapping was performed either with CARTO (Pentaray and Decanav) or with EnSite Precision (HD Grid) (Table 1). The mapping data were included in the study if the VT-SoO was identified and a sufficiently dense substrate map was produced.

Mapping was performed during ventricular pacing from the RV apex. If pacing was well tolerated, a train of 5 S_1 paced beats was delivered followed by an S_2 beat at a short coupling interval (Table 1) to

induce slow conduction necessary for RVI calculation [7]. If continuous pacing was poorly tolerated, either a train of three short coupled beats were delivered or a single paced beat was delivered shortly after sensing the R-wave of a sinus beat. In one patient with severely impaired function, biventricular pacing was delivered at a normal rate (60 bpm). The pacing procedure was continuously repeated and data collected on the post-extra systolic beat using standard criteria to enable high-density sequential mapping

In case of haemodynamically tolerated VTs, identification of VT-SoO was defined either by entrainment or by termination of VT during ablation. For unstable VTs, the VT-SoO was identified using pace mapping with an average correlation coefficient between the 12 lead ECG of VT and the paced beat ≥ 90% [11]. If multiple sites for the same VT were identified with pace mapping, the site providing the highest correlation was retained.

Ablation was delivered at the VT sites of origin and at other sites to achieve substrate modification using standard criteria [2] and was not based on RVI, which was computed off-line.

Data Analysis

Unipolar electrograms were recorded with band-pass filters set at 0.05-500 Hz and were exported along with anatomical data for bespoke off-line analysis in Matlab (Mathwork), which included stringent criteria for selecting only beats showing very similar activation/repolarization patterns (see Supplemental Methods). AT , RT and ARI were measured following standard definitions [12,13] (Figure 2) using automatic robust algorithms developed and tested during the course of previous studies [10,14–17]. Markers were revised using bespoke graphical user interfaces and semi-automatic correction, which involved performing automatic annotation within manually adjusted windows of interest. Correction was limited to isolated outliers to reduce arbitrary annotation and ensure reproducibility.

Localization of sites vulnerable to re-entry

The algorithm for RVI mapping operates as follow: For each cardiac site, neighbouring electrode sites are identified within a searching radius $R=8$ mm. The intervals between RT at a given site P and AT at neighbouring sites D, i.e. RT_P-AT_D, are measured. The shortest of these intervals represent the RVI at site P. An RVI value was thereby obtained for each electrode site in the mapped area. This process is summarized in Figure 3, where an example is provided.

For the sake of comparison, local gradients of AT, ARI and RT, which provide a quantification of local activation and repolarization heterogeneity, were also computed (Figure 3).

The distance between the VT-SoO and the nearest of the following sites was measured in order to assess the capability of localizing critical sites for VT initiation:

- Sites showing the lowest RVI, i.e. RVI < 5th percentile of RVI values. RVI ≥ 300 ms were excluded from those considered as vulnerable to re-entry even if within the lowest 5%.
- Sites showing the largest AT, RT and ARI gradients, i.e. sites for which local gradients were > the 95th percentile of their distributions.
- Sites showing the longest AT, i.e. AT > 95th percentile of AT values.
- Sites showing the longest RT and ARI, i.e. sites for which RT and ARI were > the 95th percentile of their distributions.
- Sites showing the shortest RT and ARI, i.e. sites for which RT and ARI were < the 5th percentile of their distributions.

Statistical Analysis

Data are reported as median, 1st—3rd quartiles. The Wilcoxon signed-rank test was used for comparing distances between VT-SoO and vulnerable sites identified by different markers with $P<0.05$ indicating significance.

Results

In total, 18 patients were included in the study. Baseline characteristics are reported in Table 1. Patients were aged 65, 52—70 years (median, 1st—3rd) and 16 were male. Pathologies included ischaemic heart disease (n=14, 78%) and ARVC (n=4, 22%). The cycle length of the beat preceding the mapped beat was 360, 360—398 ms and electro-anatomical maps for RVI calculation included 1012, 408—2098 unipolar electrograms (Table 1). Some patient presented more than 1 VT morphology at the time of the procedure, but in all cases the site of origin of only one VT was identified and confirmed by either entrainment (n=6) or pace mapping (n=12) (Table 1). Other VTs were not mapped either because they were thought not to be clinical or because a substrate ablation approach was preferred. This was often the case, as VT was unstable in two third of patients.

Acute VT-inducibility was tested at the end of the procedure in 12 patients (67%), while considered inappropriate in the other 6 (33%) owing to haemodynamic compromise. None of the mapped VTs was inducible at the end of the procedure, while in 2 (16%) patients a different VT morphology was induced.

During the follow-up (16.2, 7.1-20.3 months, median, minimum-maximum), 50% of patients (75% of ARVC and 43% of ischemic patients) suffered a recurrence, defined as any therapy from the implantable device, including anti-tachycardia pacing, heart transplant or death from any cause.

Assessment of RVI in relation to VT sites of origin

Figures 4A-C shows RVI maps in a patient for which the VT-SoO was identified by entrainment. The sites of lowest RVI are clustered around the VT-SoO, with the closest one being 3.1 mm away from it. Unipolar electrograms from electrode sites with large and low RVI are shown in Figure 4D-E. Figure 5A-C shows examples from another patient, where the VT-SoO was identified by pace mapping. In this case, the distance between lowest RVI sites and the VT-SoO was 3.4 mm. Some of the lowest RVI sites are distant from the VT-SoO, which is expected as these may be related to a different re-entrant circuit

from that identified during the procedure. Unipolar electrogams are shown in Figure 5D-E, with low amplitude fractionated signals recorded at site of low RVI (panel E) close to the VT-SoO.

Considering all 18 VTs, the distance between sites of lowest RVI and the VT-SoO was 5.1, 3.2—10.1 mm (median, 1^{st} – 3^{rd} quartile) (Table 1). This was not different in ischaemic and ARVC patients (4.9, 3.1-10.7 mm vs 5.2, 2.6-11.6 mm, P=0.95) or in VTs whose site of origin was identified using pace mapping vs entrainment (5.1, 4.1-9.5 mm vs 4.0, 2.5-17.9 mm, P=0.82).

Similar results were obtained using searching radius R = {7, 8, 9, 10} mm, but for smaller search radii the distance between the vulnerable region and the VT-SoO increased (Supplementary Figure 1).

Comparison between RVI and other markers in relation to VT sites of origin

The distance between the VT-SoO and lowest RVI sites was shorter than that for any other activation-repolarization marker (Figure 6). Pair-wise comparisons showed that the distance to the VT-SoO was significantly shorter for lowest RVI sites than for sites showing longest RT (P=0.020), longest ARI (P=0.004) and shortest RT (P=0.042). Despite showing the lowest median value as well as lowest standard deviation across all mapped VTs, distance to the VT-SoO from lowest RVI sites was not significantly smaller than distance to the VT-SoO from sites showing largest local gradients of AT (G_{AT}, P=0.17), ARI ($G_{ARI,}$ P=0.49), RT ($G_{RT,}$ P=0.11), or from sites showing lowest ARI (0.68) and largest AT (P=0.13) (Figure 6).

The identification of VT-SoO was considered accurate if the distance to the VT-SoO was <10 mm and inaccurate if >20 mm. RVI showed the highest accuracy, with 13 VT-SoO out of 18 located within 10 mm to lowest RVI sites (72.2%, Figure 7A) as well as the lowest inaccuracy rate, with only 1 VT-SoO located at more than 20 mm from lowest RVI sites (5.6%, Figure 7B). Inaccurate identification of VT-SoO was significantly less likely to occur for lowest RVI than for longest AT and longest ARI (odd ratio equal to 0.12, P=0.035, Chi-squared test, for both markers, Figure 7B).

Interaction between RVI and other markers

RVI showed positive correlation with ARI, cc = 0.71, 0.59—0.76, and RT, cc = 0.52, 0.23—0.72, and a weaker inverse correlation with AT, cc = -0.26, -0.45— -0.07, G_{AT}, cc = -0.25,-0.47— -0.12 and G_{ARI}, cc = -0.26, -0.44—0.09 (Supplementary Figure 2A).

Sites with lowest RVI partially overlapped with those showing shortest RT and ARI, with overlap equal to 35%, 23—42% and 24%, 12—44%, respectively (Supplementary Figure 2B). Only 5%, 0%—16% of sites with lowest RVI were also identified as vulnerable owing to longest AT. This increased to 13%, 0%—21% when considering as overlapping sites situated at a distance ≤ 2 mm. About 15% of sites showing lowest RVI also showed largest gradients of AT or ARI. This suggests that RVI captures electrophysiological vulnerability independently from standard activation-repolarization markers.

Discussion

This is the first study to use state of the art mapping technology to comprehensively evaluate the RVI and alternative activation-repolarization markers in delineating the sites critical for VT establishment. The main results are: (1) RVI identifies vulnerable regions that were within 10 mm of VT-SO in 72.2% of VTs and >20 mm away in only 5.6% of VTs, with the closest vulnerable site located 5.1, 3.2—10.1 mm from the VT-SoO. (2) Inaccurate VT-SoO identification was significantly less frequent for lowest RVI than for longest AT and longest ARI. (3) Lowest RVI identifies vulnerable regions independent of other activation and repolarization markers and it incorporates information from both local AT and ARI gradients, which identified critical regions at a (non-significantly) larger distance than lowest RVI.

RVI is based upon a conceptual model of the critical relationship between activation and repolarization restitution properties, which was formerly defined by Coronel and colleagues in an elegant animal study [6]. That study demonstrated that the critical parameter to differentiate block from the initiation of re-entrant arrhythmia was the interval between the proximal RT of the premature beat and the

arrival time of the premature wave at the distal side of the line of block. This represents the foundation of the RVI algorithm, first implemented by Taggart and colleagues in a mechanistic proof-of-principle study [7]. Results from retrospective analysis of non-contact mapping data in selective RV disorders [10] and computational studies [8,9] have provided support to the validity of the RVI concept. This study has assessed for the first time the RVI as a potential clinical tool to identify critical targets for ablation by utilising state of the art mapping technology in both RV and LV pathologies and comparing it to other activation-repolarization metrics of functional substrate. The results suggest that RVI could represent a useful metric to inform novel substrate ablation strategies.

While other studies have focused on improving the delineation of the arrhythmogenic substrate with late potentials [18,19], metrics related to slow conduction, visualization of potential diastolic pathway and characterization of channels using imaging [2,20], this study demonstrates that repolarization is critical for the identification of VT-SoO.

RVI performed similarly to, but independently of, local gradients of activation, an established marker of arrhythmia susceptibility [21], which is embedded in the RVI concept. A moderate correlation between RVI and local activation and repolarization gradients confirms the theoretical observation that RVI integrates information from both activation and repolarization dynamics.

Current performance and future developments

Despite its solid theoretical underpinning, RVI was not significantly superior to other markers in the identification of the VT-SoO. This may be partially due to lack of statistical power (n=18) and both procedural and technological limitations. A critical aspect of RVI is the pacing protocol, with both cycle length and pacing site potentially affecting RVI maps [8]. The importance of stimulating the tissue at a coupling interval short enough to engage conduction velocity restitution to unmask electrophysiological vulnerability is well recognised [19]. It may be possible that a more aggressive S_1S_2 pacing protocol could have provided more precise localisation but at the risk of haemodynamic compromise and VT induction in these vulnerable patients. The pacing site affects both voltage [22] and

activation-repolarization properties [23] and pacing from multiple sites may improve RVI delineation of the arrhythmogenic substrate [8]. This was not feasible due to time constraints during the procedure.

Importantly, in structurally abnormal hearts, multiple pathways may support different VTs, some of which may not be revealed during the procedure. This limits the extent by which any metric theoretically related to sites susceptible to re-entry can be validated using information from the VTs mapped during the procedure. Validation by prospective studies using ablation to target all low RVI sites will be required in randomised controlled trials to test this physiological mapping approach versus current VT ablation strategies to determine VT recurrence, hospitalisations and mortality.

Limitations

Although bespoke software solutions were implemented to analyse only beats with the same activation-repolarization sequence and semi-automatic correction was kept to a minimum to ensure reproducibility, repolarization variability during sequential mapping and the challenge of measuring activation/repolarization markers in diseased myocardium may have affected the results. Ultra-fast non-contact mapping providing AT and RT within one single beat may represent a possible solution [24].

The identification of VT-SoO with pacing manoeuvres presents limitations inherent to electro-anatomical mapping. Pace-mapping is a standard approach to identify the exit site of unstable VTs [11], but its accuracy can be affected by area of capture and functional block only present in VT. A previous study has reported 82% sensitivity and 87% specificity in identifying the exit region by pace mapping with a 82% morphology match [11]. Our cut-off value of 90% morphology match should provide slightly higher specificity. Although none of the mapped VTs were inducible after ablation, acute VT induction could not be consistently tested as procedural end-point owing to hemodynamic compromise in 6 patients. The recurrence rate was 50% after a median follow-up of 16 months, which is in line with other studies [1]. This is likely due to limitations of current ablation strategies in complex patients with haemodynamic compromise and presenting multiple potential vulnerable sites for VT development most of which are concealed at the time of the procedure and cannot be localized with entrainment,

pace-mapping or standard substrate mapping. This study did not set out to prospectively ablate low RVI sites, which will be the subject of future studies to assess whether this influences outcomes.

Conclusions

These data show that RVI identifies vulnerable regions that closely correlate with the VT site of origin and suggest that activation-repolarization metrics may improve the delineation of the arrhythmogenic substrate and enable optimal substrate based ablation without the risks of compromising the patient with multiple VT inductions.

Acknowledgements

FOC, MJB and BMH acknowledge the support of the British Heart Foundation through Project Grant PG/16/81/32441. PDL is supported by UCLH Biomedicine NIHR and Barts BRC, Stephen Lyness Research Fund.

References

1. Shivkumar K: Catheter Ablation of Ventricular Arrhythmias. Jarcho JA, ed: N Engl J Med Massachusetts Medical Society, 2019; 380:1555–1564.

2. Santangeli P, Marchlinski FE: Substrate mapping for unstable ventricular tachycardia. Heart Rhythm Elsevier, 2016; 13:569–583.

3. Bourier F, Martin R, Martin CA, et al.: Is it feasible to offer “targeted ablation” of ventricular tachycardia circuits with better understanding of isthmus anatomy and conduction characteristics? Europace Narnia, 2019; 21:I27–I33.

4. Josephson ME, Anter E: Substrate Mapping for Ventricular Tachycardia. JACC Clin Electrophysiol 2015; 1:341–352.

5. Mines GR: On dynamic equilibrium in the heart. J Physiol Wiley-Blackwell, 1913; 46:349–383.

6. Coronel R, Wilms-Schopman FJG, Opthof T, Janse MJ: Dispersion of repolarization and arrhythmogenesis. Heart Rhythm 2009; 6:537–543.

7. Child N, Bishop MJ, Hanson B, et al.: An activation-repolarization time metric to predict localized regions of high susceptibility to reentry. Heart Rhythm 2015; 12:1644–1653.

8. Hill YR, Child N, Hanson B, Wallman M, Coronel R, Plank G, Rinaldi CA, Gill J, Smith NP, Taggart P, Bishop MJ: Investigating a novel activation-repolarisation time metric to predict localised Vulnerability to reentry using computational modelling. PLoS One Public Library of Science, 2016; 11:e0149342.

9. Campos FO, Orini M, Taggart P, Hanson B, Lambiase PD, Porter B, Rinaldi CA, Gill J, Bishop MJ: Characterizing the clinical implementation of a novel activation-repolarization metric to identify targets for catheter ablation of ventricular tachycardias using computational models. Comput Biol Med Pergamon, 2019; 108:263–275.

10. Martin CA, Orini M, Srinivasan NT, Bhar-Amato J, Honarbakhsh S, Chow AW, Lowe MD, Ben-Simon R, Elliott PM, Taggart P, Lambiase PD: Assessment of a conduction-repolarisation metric to predict Arrhythmogenesis in right ventricular disorders. Int J Cardiol 2018; 271:75–80.

11. De Chillou C, Groben L, Magnin-Poull I, et al.: Localizing the critical isthmus of postinfarct ventricular tachycardia: The value of pace-mapping during sinus rhythm. Heart Rhythm Elsevier, 2014; 11:175–181.

12. Coronel R, de Bakker JMT, Wilms-Schopman FJG, Opthof T, Linnenbank AC, Belterman CN, Janse MJ: Monophasic action potentials and activation recovery intervals as measures of ventricular action potential duration: Experimental evidence to resolve some controversies. Heart Rhythm 2006; 3:1043–1050.

13. Orini M, Srinivasan NT, Graham A, Taggart P, Lambiase P: Further evidence on how to measure

311 local repolarization time using intracardiac unipolar electrograms in the intact human heart.
312 Circ Arrhythm Electrophysiol 2019; .

313 14. Orini M, Taggart P, Lambiase PD: In vivo human sock-mapping validation of a simple model that
314 explains unipolar electrogram morphology in relation to conduction-repolarization dynamics.
315 J Cardiovasc Electrophysiol 2018; 29:990–997.

316 15. Orini M, Taggart P, Srinivasan N, Hayward M, Lambiase PD: Interactions between activation
317 and repolarization restitution properties in the intact human heart: In-vivo whole-heart data
318 and mathematical description. PLoS One 2016; 11:e0161765.

319 16. Orini M, Yanni J, Taggart P, et al.: Mechanistic insights from targeted molecular profiling of
320 repolarization alternans in the intact human heart. Europace 2019; 21:981–989.

321 17. Orini M, Citi L, Hanson BMBM, Taggart P, Lambiase PDPDPD: Characterization of the causal
322 interactions between depolarization and repolarization temporal changes in unipolar
323 electrograms. Computing in Cardiology IEEE, 2013, pp. 719–722.

324 18. Vergara P, Trevisi N, Ricco A, Petracca F, Baratto F, Cireddu M, Bisceglia C, Maccabelli G, Della
325 Bella P: Late potentials abolition as an additional technique for reduction of arrhythmia
326 recurrence in scar related ventricular tachycardia ablation. J Cardiovasc Electrophysiol John
327 Wiley & Sons, Ltd (10.1111), 2012; 23:621–627.

328 19. Porta-Sánchez A, Jackson N, Lukac P, et al.: Multicenter Study of Ischemic Ventricular
329 Tachycardia Ablation With Decrement-Evoked Potential (DEEP) Mapping With Extra Stimulus.
330 JACC Clin Electrophysiol Elsevier, 2018; 4:307–315.

331 20. Sramko M, Hoogendoorn JC, Glashan CA, Zeppenfeld K: Advancement in cardiac imaging for
332 treatment of ventricular arrhythmias in structural heart disease. Europace 2019; 21:383–403.

333 21. Ciaccio EJ, Chow AW, Davies DW, Wit AL, Peters NS: Localization of the Isthmus in Reentrant
334 Circuits by Analysis of Electrograms Derived from Clinical Noncontact Mapping during Sinus

Rhythm and Ventricular Tachycardia. J Cardiovasc Electrophysiol John Wiley & Sons, Ltd (10.1111), 2004; 15:27–36.

22. Tung R, Josephson ME, Bradfield JS, Shivkumar K: Directional Influences of Ventricular Activation on Myocardial Scar Characterization: Voltage Mapping with Multiple Wavefronts during Ventricular Tachycardia Ablation. Circ Arrhythmia Electrophysiol 2016; 9.

23. Srinivasan NT, Orini M, Simon RB, et al.: Ventricular stimulus site influences dynamic dispersion of repolarization in the intact human heart. Am J Physiol - Hear Circ Physiol 2016; 311:H545–H554.

24. Graham AJ, Orini M, Zacur E, et al.: Simultaneous Comparison of Electrocardiographic Imaging and Epicardial Contact Mapping in Structural Heart Disease. Circ Arrhythm Electrophysiol 2019; 12:e007120.

Tables

	Sex	Age (years)	Aetiology	VT-SoO	EAM	Catheter	Pacing Interval (ms)	Pacing Type	Points on Map (n)	Dist to VT-SoO (mm)
1	M	69	IHD	PM	CARTO	Pentaray	500	S1S1	4190	8.3
2	F	34	ARVC	ENT	CARTO	Pentaray	460	S1S1	2256	17.9
3	M	71	IHD	PM	CARTO	Pentaray	360	S1S2	2560	4.9
4	F	52	ARVC	PM	CARTO	Pentaray	360	S1S1	1312	5.2
5	M	79	IHD	ENT	CARTO	Pentaray	380	S1S2	260	4.8
6	M	55	IHD	PM	CARTO	Pentaray	360	S1S2	1625	8.2
7	M	70	IHD	PM	CARTO	Pentaray	360	S1S2	370	16.5
8	M	73	ARVC	PM	CARTO	Pentaray	360	S1S2	328	5.2
9	M	22	ARVC	PM	CARTO	Decanav	1000	$S1S1^{BV}$	4325	0.0
10	M	65	IHD	ENT	Precision	HD-Grid	360	SE	1341	33.9
11	M	68	IHD	PM	Precision	HD-Grid	360	SE	1304	13.8
12	M	50	IHD	PM	Precision	HD-Grid	360	SE	4328	10.7
13	M	61	IHD	ENT	Precision	HD-Grid	325	SE	719	1.9
14	M	65	IHD	PM	Precision	HD-Grid	360	S1S2	356	3.4
15	M	77	IHD	PM	Precision	HD-Grid	400	SE	389	5.0
16	M	60	IHD	PM	Precision	HD-Grid	390	SE	466	1.7
17	M	52	IHD	ENT	Precision	HD-Grid	360	SE	511	3.1
18	M	65	IHD	ENT	Precision	HD-Grid	400	SE	667	2.5
	89% M	65 (53-70)	72% IHD	67% PM	50% CARTO	50% HD-Grid	360 (360-398)	44% SE	1012 (408-2098)	5.1 (3.2-10.1)

Table 1: Patient's information. IHD: ischemic heart disease; ARVC: Arrythmogenic Right Ventricular Cardiomyopathy. Pacing manoeuvres to determine the VT site of origin, VT-SoO, were either entrainment (ENT) or pace mapping (PM). Electro-anatomical mapping systems were CARTO or Ensite Precision. Pacing types were S1S1, S1S2 or sensed-extras (SE). $S1S1^{BV}$ denotes bi-ventricular pacing. Points on Map is the number of unipolar electrograms per map. Dist to VT-SoO is the distance between the VT site of origin and the nearest site showing lowest RVI.

Figures

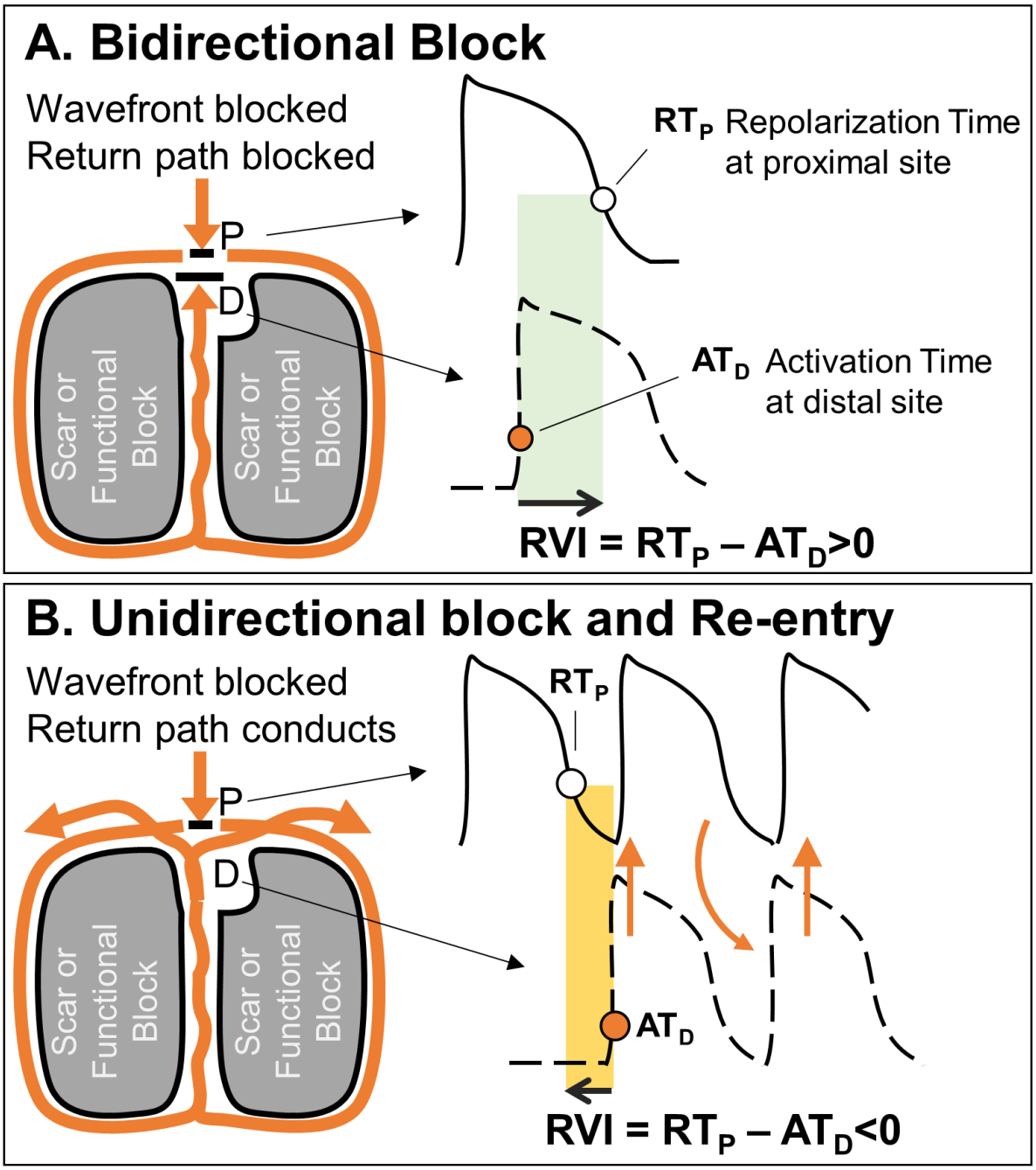

Figure 1: Theoretical model underpinning the re-entry vulnerability index (RVI). See text. Similar diagrams can be found in [6,7,10].

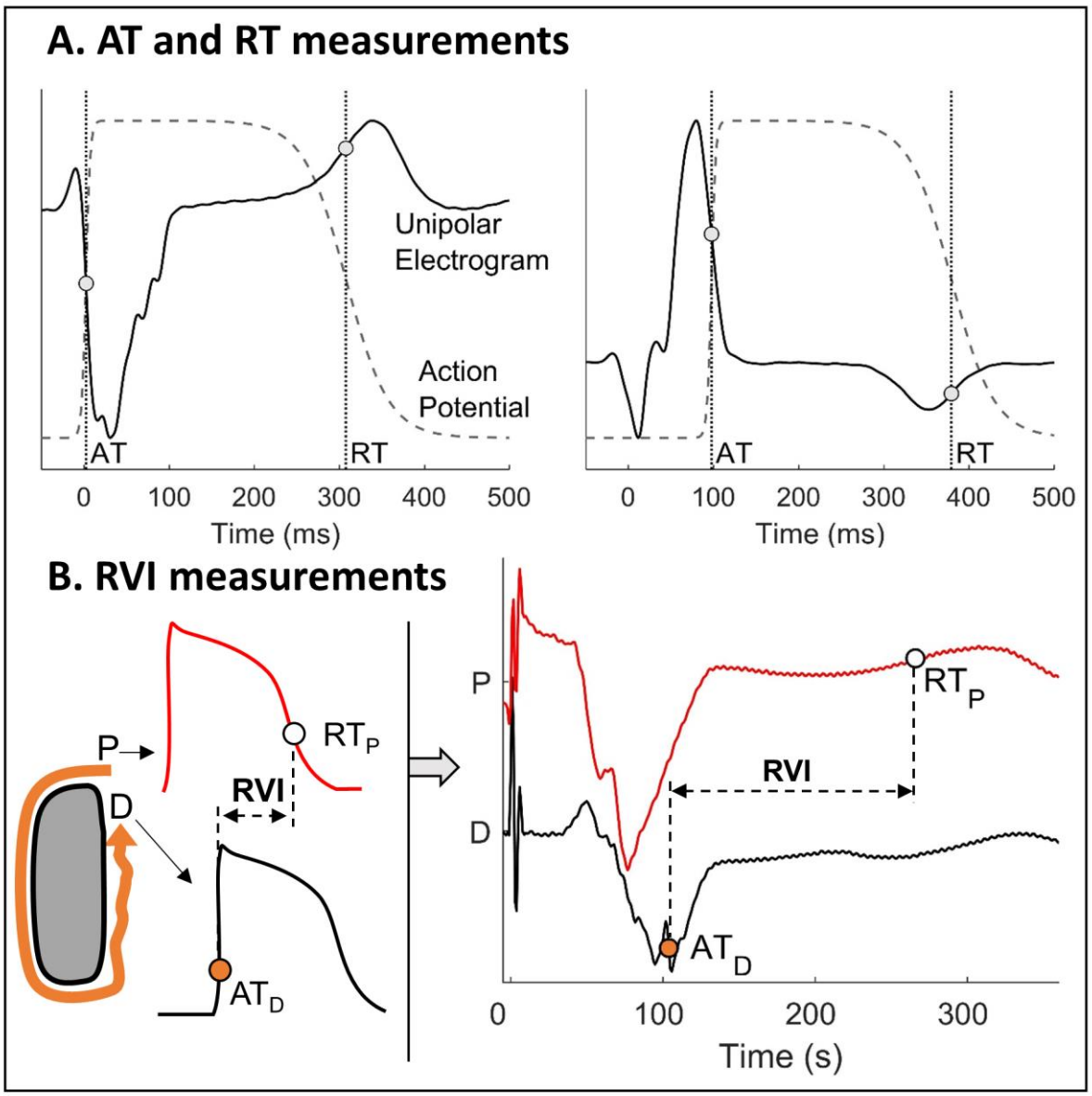

362

363 **Figure 2**: **Computation of spatial activation-repolarization metrics.** A: Stylised action
364 potentials and unipolar electrograms showing standard measurements of activation (AT) and
365 repolarization (RT) times. B: Conceptual model for RVI measurement (left) and RVI
366 measurements using recorded unipolar electrograms (right).

367

368

369

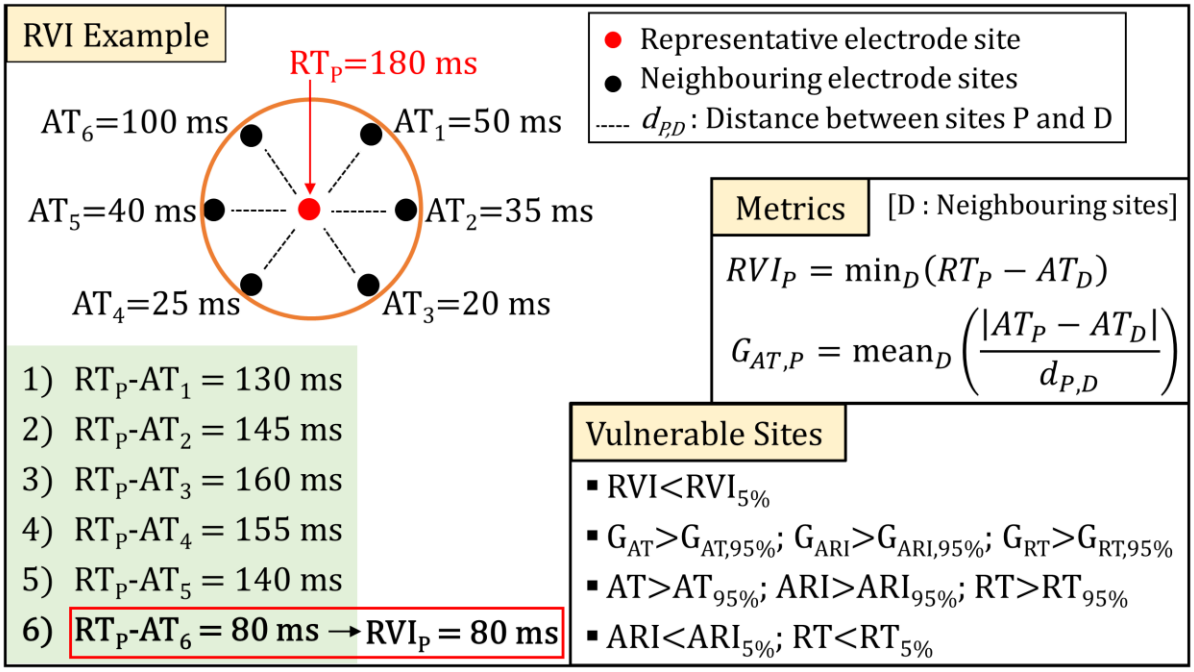

Figure 3: Computation of RVI and spatial activation-repolarization metrics. Left: The red dot represents a cardiac site P for which RVI is measured. Black dots represent neighbouring cardiac sites within a searching radius R. As shown in the example in the box, RVI is the shortest interval between AT at neighbouring sites and RT at site P, RT_P-AT_D. The formula for RVI and local gradients measurement are reported on the right. Local gradients of ARI and RT are measured in the same way. The criteria for identifying vulnerable sites to re-entry are given in the bottom-right panel.

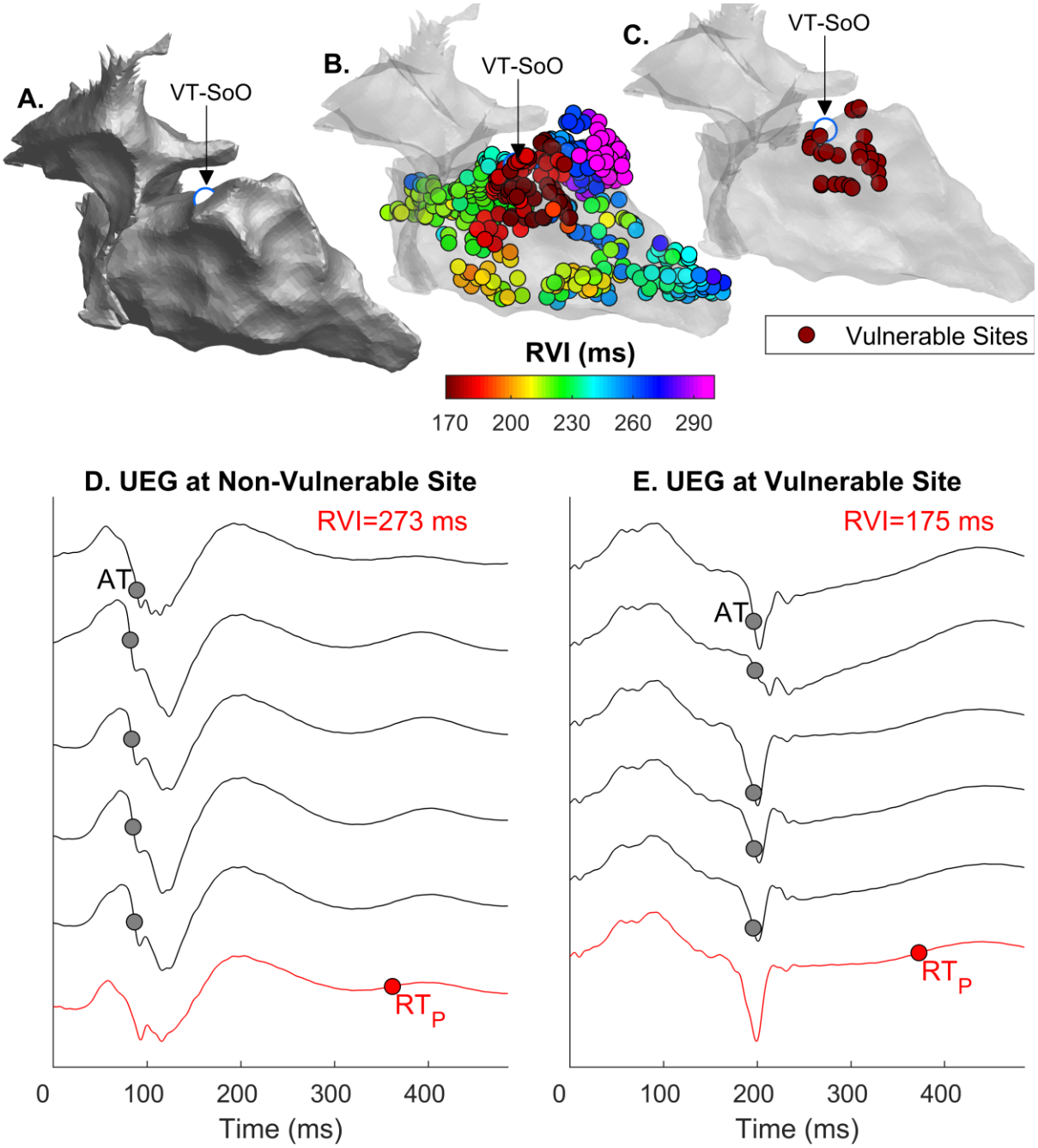

379

380 **Figure 4: Example of RVI identifying vulnerable sites close to an entrained VT.** A: Anatomical map
381 showing the VT site of origin (VT-SoO) as a white dot. B: RVI map where each dot represents a cardiac
382 site and RVI is colour-coded. C: map showing sites showing the lowest 5% of RVI values. D-E: Unipolar
383 electrograms from an electrode site showing high (D) and low (E) RVI (red line) and from neighbouring
384 electrode sites (grey). Red and grey circles represent RT at the site of RVI measurement, RT_P, and AT
385 at neighbouring sites, respectively.

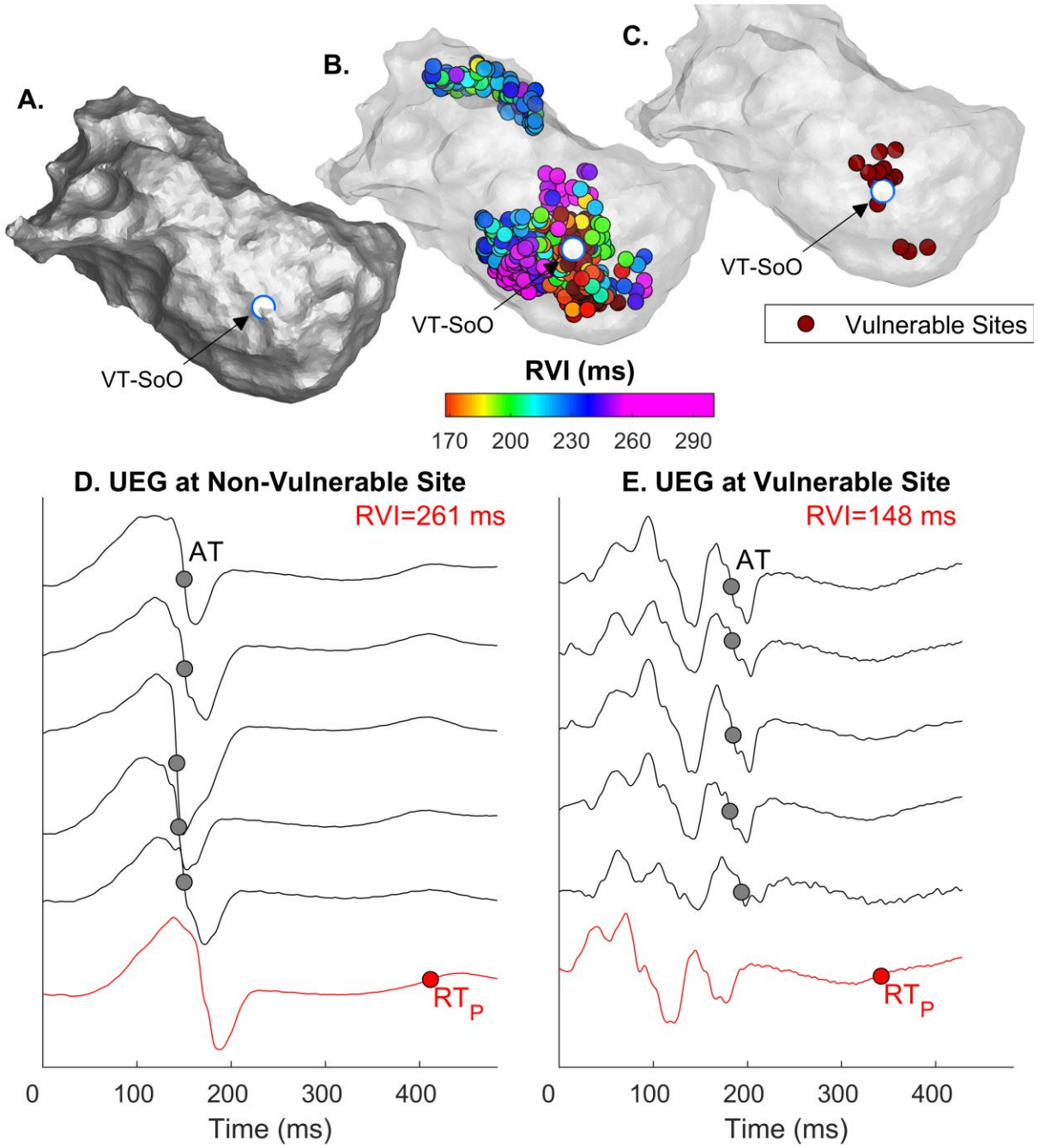

Figure 5: Example of RVI identifying vulnerable sites close to a pace-mapped VT. See Figure 4's legend for details.

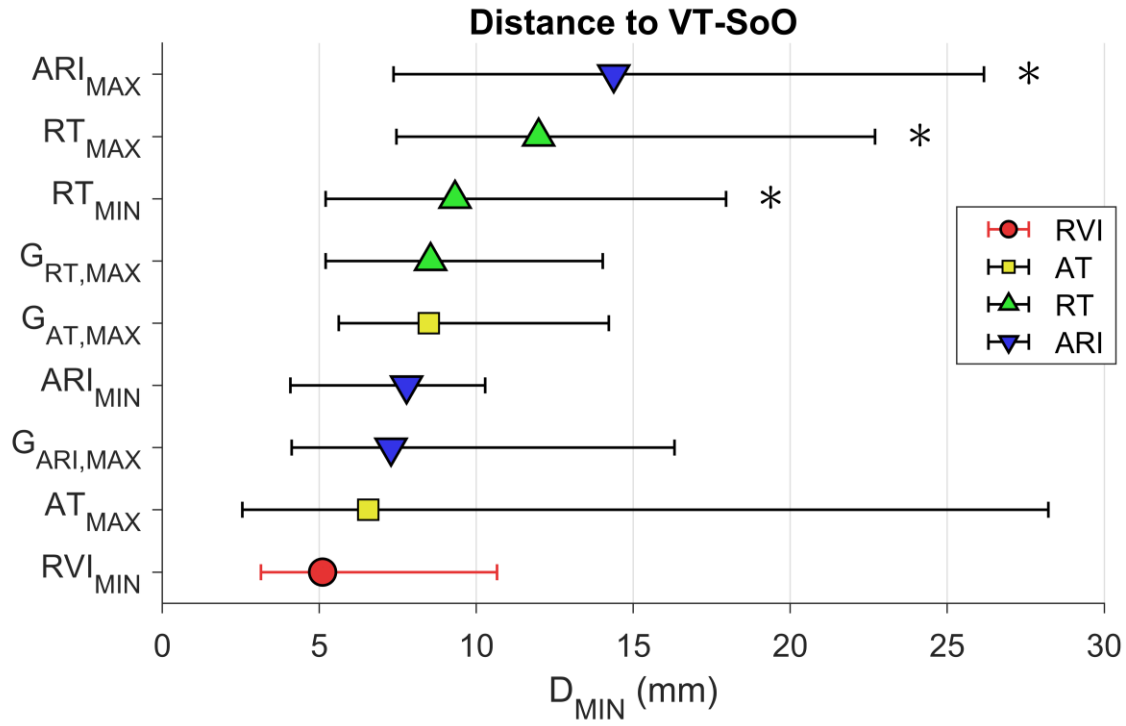

Figure 6: Distance to VT site of origin. Distance between the VT site of origin (VT-SoO) and nearest vulnerable sites identified by lowest RVI (RVI_{MIN}), largest gradients of AT ($G_{AT,MAX}$), largest gradients of RT ($G_{RT,MAX}$), largest gradients of ARI ($G_{ARI,MAX}$), longest AT (AT_{MAX}), shortest RT (RT_{MIN}), longest RT (RT_{MAX}), shortest ARI (ARI_{MIN}) and longest ARI (ARI_{MAX}). Markers indicate the median of minimum distances and bars span the 1st—3rd quartile interval (across n=18 VTs). *: P<0.05 with respect to RVI_{MIN}..

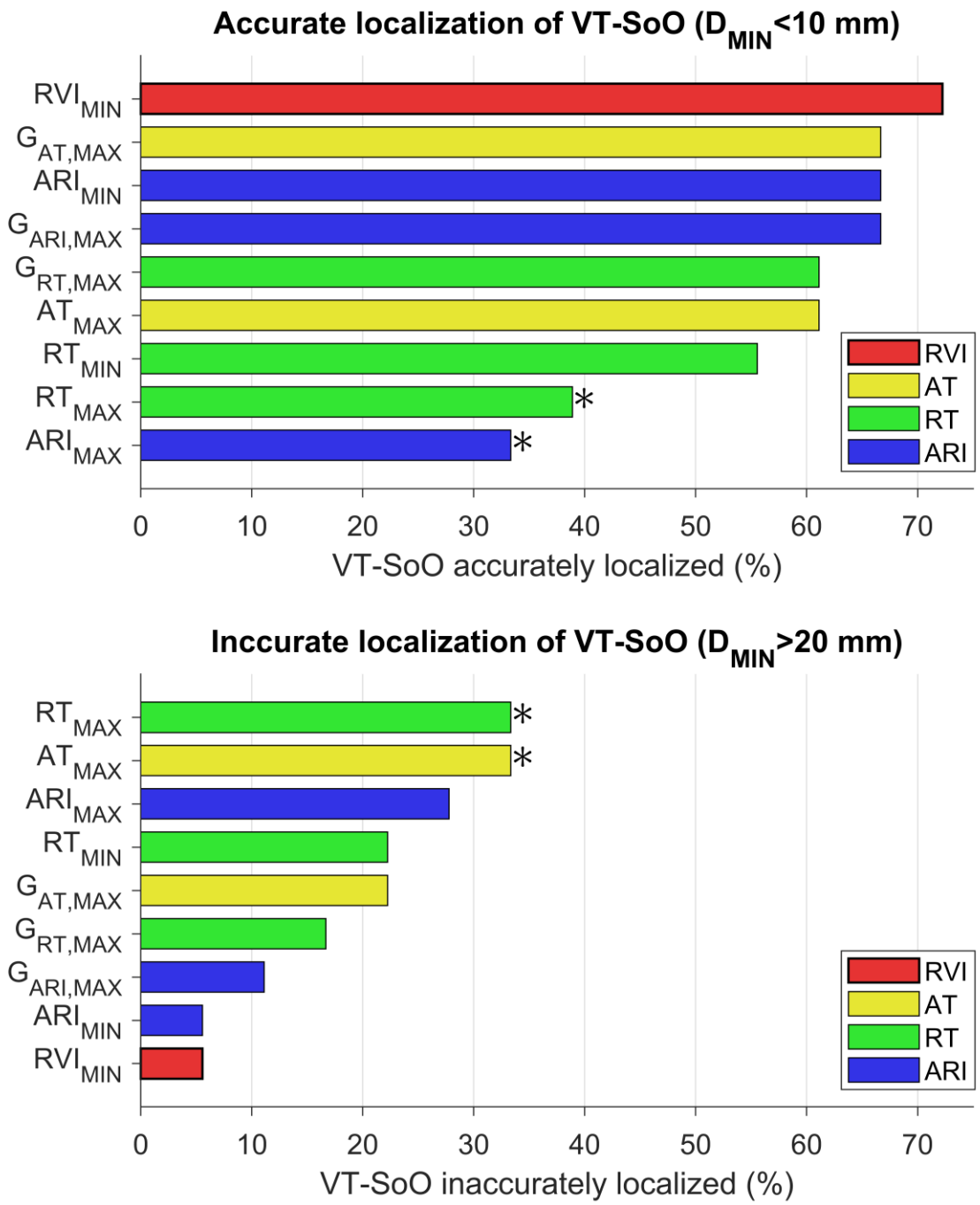

401

402 **Figure 7: Accuracy of VT sites of origin localization.** Proportion of VTs for which the distance between

403 VT-SoO and the vulnerable sites was <10 mm (A, accurate localization of VT-SoO). >20 mm (B,

404 inaccurate localization of VT-SoO). * : P<0.05 with respect to RVI_{MIN}.

405